# the plant journal



The Plant Journal (2023) 116, 756-772

doi: 10.1111/tpj.16403

# AXR1 modulates trichome morphogenesis through mediating ROP2 stability in Arabidopsis ©

Lu Liu<sup>1</sup>, Linyu Niu<sup>1</sup>, Ke Ji<sup>1</sup>, Yali Wang<sup>1</sup>, Chi Zhang<sup>1</sup>, Mi Pan<sup>1</sup>, Wenjia Wang<sup>2</sup>, John Schiefelbein<sup>3</sup>, Fei Yu<sup>1</sup> and Lijun An<sup>1,\*</sup> Distance Key Laboratory of Crop Stress Biology for Arid Areas and College of Life Sciences, Northwest A&F University, Yangling, Shaanxi 712100, China,

<sup>2</sup>CAS Center for Excellence in Molecular Plant Sciences, Chinese Academy of Sciences, Shanghai 200032, China, and <sup>3</sup>Department of Molecular, Cellular, and Developmental Biology, University of Michigan, Ann Arbor, Michigan 48109, USA

Received 6 December 2022; revised 9 July 2023; accepted 17 July 2023; published online 30 July 2023. \*For correspondence (e-mail lijunan@nwsuaf.edu.cn).

#### **SUMMARY**

Cell differentiation and morphogenesis are crucial for the establishment of diverse cell types and organs in multicellular organisms. Trichome cells offer an excellent paradigm for dissecting the regulatory mechanisms of plant cell differentiation and morphogenesis due to their unique growth characteristics. Here, we report the isolation of an Arabidopsis mutant, aberrantly branched trichome 3-1 (abt3-1), with a reduced trichome branching phenotype. Positional cloning and molecular complementation experiments confirmed that abt3-1 is a new mutant allele of Auxin resistant 1 (AXR1), which encodes the N-terminal half of ubiquitin-activating enzyme E1 and functions in auxin signaling pathway. Meanwhile, we found that transgenic plants expressing constitutively active version of ROP2 (CA-ROP2) caused a reduction of trichome branches, resembling that of abt3-1. ROP2 is a member of Rho GTPase of plants (ROP) family, serving as versatile signaling switches involved in a range of cellular and developmental processes. Our genetic and biochemical analyses showed AXR1 genetically interacted with ROP2 and mediated ROP2 protein stability. The loss of AXR1 aggravated the trichome defects of CA-ROP2 and induced the accumulation of steadystate ROP2. Consistently, elevated AXR1 expression levels suppressed ROP2 expression and partially rescued trichome branching defects in CA-ROP2 plants. Together, our results presented a new mutant allele of AXR1, uncovered the effects of AXR1 and ROP2 during trichome development, and revealed a pathway of ROP2-mediated regulation of plant cell morphogenesis in Arabidopsis.

Keywords: AXR1, genetic interaction, protein stability, ROP GTPase, trichome branching.

#### INTRODUCTION

Cell morphogenesis is critical for the proper establishment of plant tissue and organ shapes as well as their biological properties. Trichomes are accessorial structures that differentiate from the epidermis of the aerial parts of most plants, and their morphology varies considerably among species (Chalvin et al., 2020; Wang et al., 2019). The species-specific trichome characteristics not only play important roles for their ecological functions and economic values (Li et al., 2022; Matias-Hernandez et al., 2017; Zhang et al., 2011) but also are very useful in plant cell biology (Hülskamp, 2004; Robinson & Roeder, 2015). In Arabidopsis, the leaf trichome is single celled structure, consisting of a stalk that protrudes from the epidermal plane and usually crowned by 3 or 4 branches (Hülskamp et al., 1994; Schwab et al., 2000). During the past thirty years, the underlying regulatory mechanisms for formation of such an exquisite structure have been extensively studied (Fambrini & Pugliesi, 2019; Han et al., 2022; Wang et al., 2021).

Auxin resistant 1 (AXR1) was initially isolated in an effort to identify genes involved in auxin-mediated growth and development (Estelle & Somerville, 1987; Lincoln et al., 1990). Further studies indicate that AXR1 plays a pivotal role in auxin signaling transduction (del Pozo, Boniotti, et al., 2002; del Pozo, Dharmasiri, et al., 2002; Leyser et al., 1993). One common mechanism for auxin to orchestrate the diverse developmental processes is via regulating of gene expression through the TIR1/AFB-AUX/IAA signaling system (Leyser, 2018). In this mechanism, auxin is perceived by the Transport inhibitor response 1 (TIR1), which is an F-box protein and can interact with ASK1 and Cullin protein to form an ASK1-Cullin-TIR1 (SCF<sup>TIR1</sup>) E3 ubiquitin ligase (Gray et al., 1999; Ruegger et al., 1998). The participation of AXR1 in auxin signaling transduction is mainly

through the RUB modification of Cullin protein (del Pozo, Boniotti, et al, 2002; del Pozo, Dharmasiri, et al., 2002). AXR1 protein is related to the N-terminal half of ubiquitinactivating enzyme and can interact with ECR1 to form a bipartite enzyme to activate RUB1 (Leyser et al., 1993). The activated RUB1 will then be conjugated to the Cullin protein to activate the SCFTIR1 E3 ligase activity (Gray et al., 1999; Ruegger et al., 1998). Consistently, axr1 mutants exhibit diminished response to auxin and produce pleiotropic morphological defects in essentially all processes thought to be mediated by auxin (Estelle & Somerville, 1987; Lincoln et al., 1990).

Rho-related GTPase of plants (ROPs) are a distinct subfamily of Rho GTPase from plants (Nagawa et al., 2010). As molecular switches, ROPs take part in a plethora of cellular and developmental processes (Li et al., 2001; Liu et al., 2021; Ou & Yi, 2022; Yang et al., 2019) and most conspicuous in establishing the interdigitated jigsaw-puzzle appearance of leaf and cotyledon pavement cells (Liu et al., 2021). The Arabidopsis genome contains 11 ROPs, termed ROP1-ROP11, and whose distributions and activities of these genes are regulated by various factors (Chai et al., 2016; Igisch et al., 2022; Liu et al., 2021). Trace exogenous auxin treatment could activate ROP2 and ROP6 within 30 sec, and such a rapid response depend on an auxin/ABP1-TMK1/ROP2 signaling transduction pathway (Xu et al., 2010, 2014). Auxin binding protein 1 (ABP1) perceives extracellular auxin and then interacts with Transmembrane Kinase 1 (TMK1) at the cell surface to form an auxin sensing complex to activate ROP signaling in an auxin dose-dependent manner (Friml et al., 2022; Gao et al., 2015; Li et al., 2021; Lin et al., 2021; Xu et al., 2010, 2014; Yu et al., 2022). The activity of ROP2 is also regulated at the post-translational level. Pluripetala (PLP) encodes the shared  $\alpha$  subunit of two heterodimeric protein isoprenyltransferases, mediating 26S proteasome dependent ROP2 degradation (Chai et al., 2016). Loss of PLP function resulted in cytoplasmic accumulation of ROP2 in root hair and reduced its stability (Chai et al., 2016). Although these lines of evidence imply new clues to the regulation of ROPs activities, the mechanisms that underlie the degradation, in particular, whether a similar mechanism independently while parallelly control of ROP stability by PLP, exists in other developmental and cellular processes remains obscure.

In this study, we showed that AXR1 is required for trichome morphogenesis in Arabidopsis and functional loss of AXR1 inhibits trichome branching. Further, we observed CA-ROP2 mutants and ROP2 overexpression plants also display trichomes with reduced branches, which was resembled to axr1 mutants. Genetic and biochemical investigations uncovered an AXR1-ROP2 pathway in regulating trichome cell development. AXR1 mutation could enhance the trichome phenotypes of CA-ROP2, and more importantly, affect the stability of ROP2, resulting the

accumulation of ROP2. Taken together, by using the trichome cell as a model system, we have characterized the effects of AXR1 and ROP2 in trichome morphogenesis and identified a new ROP2 signaling process in Arabidopsis.

# **RESULTS**

# The loss of AXR1 leads to reduced trichome branching in **Arabidopsis**

To identify new genetic factors that govern trichome development, we generated an ethyl methanesulfonate (EMS)-mutagenesis population in Arabidopsis gl2-3 mutant background (salk\_039825, Wang et al., 2010) and performed screens for additional mutants with altered trichome phenotypes. During the process, a recessive mutant, designated as aberrantly branched trichome 3–1 (abt3-1), was isolated. The abt3-1 mutant displayed pleiotropic developmental defects, including reduced plant stature and apical dominance, wrinkled leaves, and shorter and less root hairs (Figure 1a,b; Figure S1). More importantly, the trichome branching was also affected in abt3-1. Under our growth conditions, the majority of leaf trichomes were three-( $\sim$ 74%) or four-branched ( $\sim$ 26%) on the 3rd rosette leaves of wild type (WT) plants, while two- or less branched trichomes were rare (Figure 1c,d). In contrast, the proportion of three-branched trichomes reached  $\sim\!96\%$  on the 3rd rosette leaves of abt3-1, and four-branched trichomes were almost absent (  $\sim$  0.74%, Figure 1c,d). Moreover, some twobranched trichomes ( $\sim$ 4%) were observed in abt3-1 (Figure 1c,d). We also compared the trichome branching differences on the 4th rosette leaves between the WT and the abt3-1 mutant, and obtained similar results as those on the 3rd rosette leaves (Figure 1e), suggesting that the trichome phenotypes in abt3-1 are not developmentally associated. Thus, the trichome branching phenotypes of the 3rd rosette leaves were employed in subsequent analyses. Taken together, these data indicate that functional loss of ABT3 inhibits trichome branching and ABT3 functions as an important positive regulator of trichome branching as well as of plant development.

To reveal the molecular nature of ABT3, we cloned the ABT3 locus through map-based cloning. Initial bulked segregant analyses linked the ABT3 locus to the molecular markers T25N20 and F316 on chromosome I (Figure 2a; Figure S2). Further fine mapping located the abt3-1 mutation to an interval upstream of T25N20 (Figure 2a). Literature search revealed the presence of the Auxin resistant 1 (AXR1, AT1G05180) gene in this region, whose loss-offunction mutants display developmental defects resembling that of the abt3-1 mutant (Estelle & Somerville, 1987; Lincoln et al., 1990). To test whether mutation in AXR1 renders the developmental defects of abt3-1, the genomic region of AXR1 in abt3-1 was sequenced and a single nucleotide transition of G-to-A was revealed in the 4th

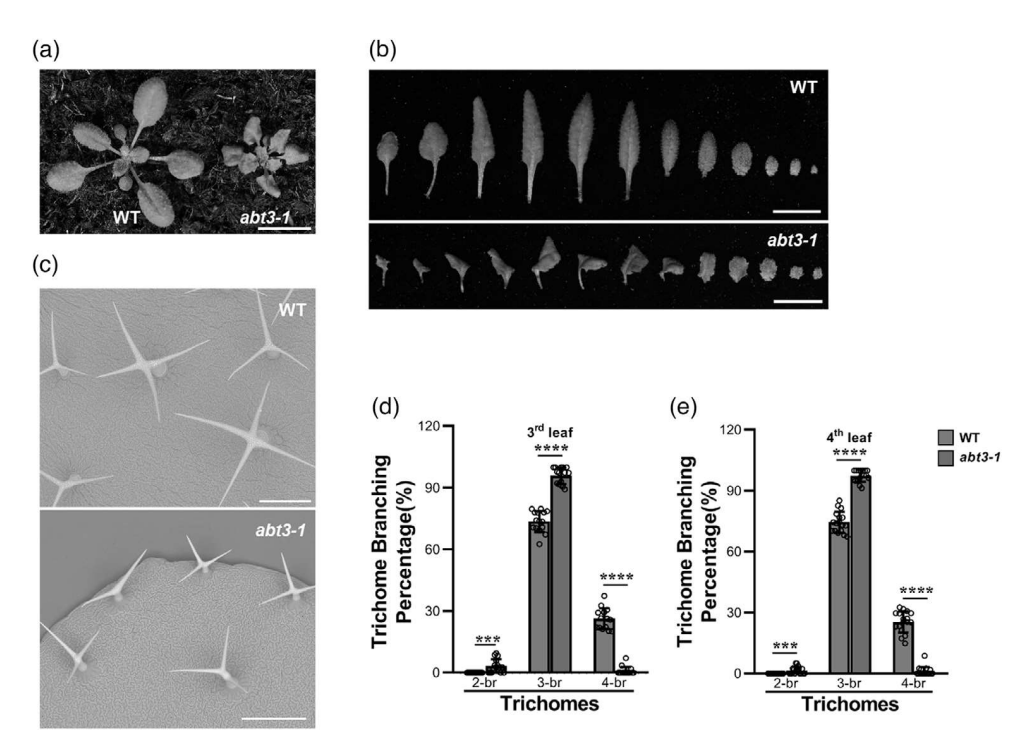


Figure 1. Phenotypes of the wild type and *abt3-1* plants.
(a) The overall growth phenotypes of 2-week-old wild type (WT) and *abt3-1*. Scale bar = 1 cm.
(b) Leaf morphologies of 3-week-old WT and *abt3-1*. *abt3-1* showed smaller and wrinkled leaves compared that in WT. Scale bars = 1 cm.
(c) Representive trichomes on the fifth rosette leaves of 3-week-old WT and *abt3-1*. Scale bars = 250 μm.
(d,e) Quantification of the trichome branch numbers of WT and *abt3-1* on the third (c) and fourth rosette leaves (d). 2/3/4-br for two/three/four-branched trichomes, respectively. Data were presented as mean ± SD. Student's *t*-test was used to assess the difference from WT (\*\*\*\*, *P* < 0.001; \*\*\*\*\*, *P* < 0.0001).

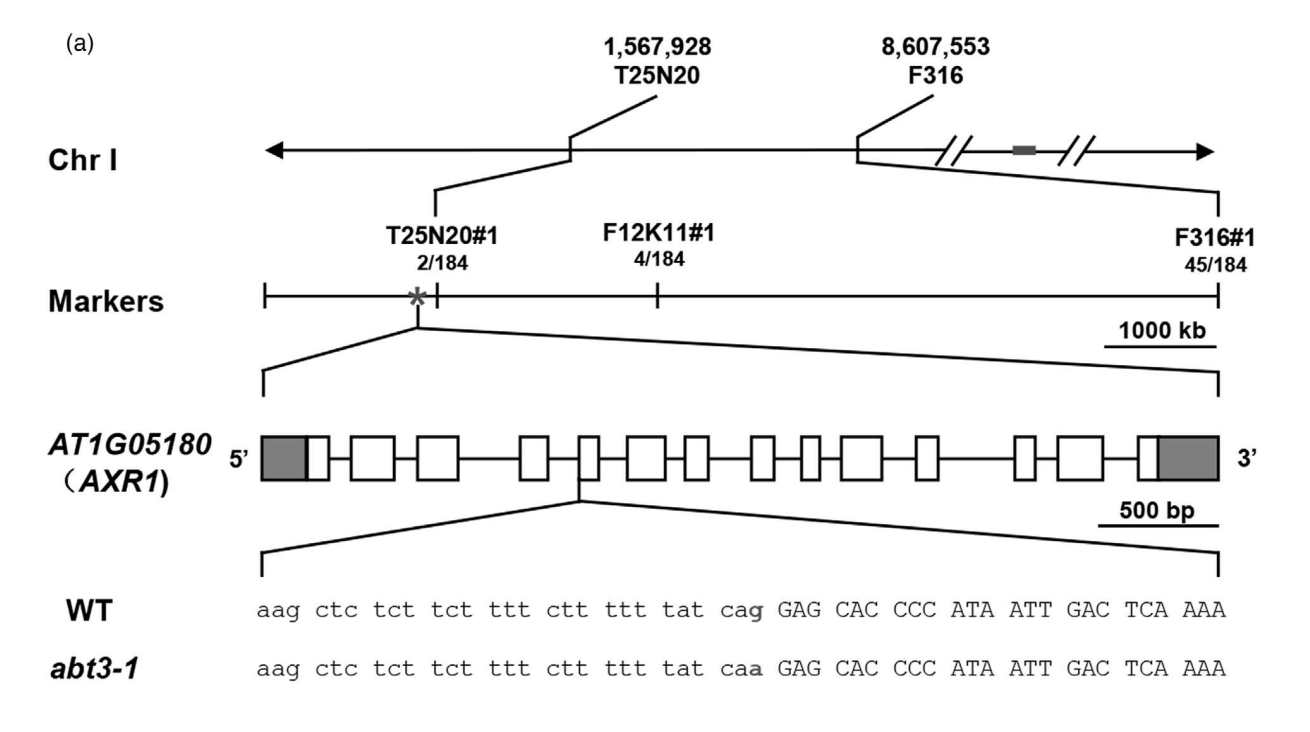
intron of the AXR1 gene (Figure 2a). Since this mutation happened to alter the conserved GA-AG sequence module which is required for RNA splicing (Shang et al., 2017), theoretically it would lead to the aberrant splicing of AXR1 transcripts. In consistent, we found that the expression level of AXR1 was remarkably reduced in abt3-1 (Figure 2d). To verify if abt3-1 represents a new mutant allele of AXR1, we carried out allelic tests using another mutant allele of AXR1, axr1-3 (Figure S3a; Lincoln et al., 1990). The overall growth and development of axr1-3 was similar to that of abt3-1 (Figure S3b-d), and abt3-1 showed severer phenotypes (Figure S3b-d). Consistently, examination and quantification of trichome branching on the 3rd rosette leaves of axr1-3 also showed a hypobranched trichome phenotype as that in abt3-1, although which is slight weaker than abt3-1 (Figure S3e-g). The F1 plants of a cross between abt3-1 and axr1-3 showed similar phenotypes to both abt3-1 and axr1-3 plants in the overall growth morphologies as well as trichome phenotypes (Figure S3b-f), indicating that abt3-1 failed to complement axr1-3, and ABT3 likely represents the same genetic locus as AXR1. We also performed molecular complementation tests by introducing the coding sequence of AXR1 driven by its own promoter into the abt3-1 mutant background

and generating *abt3-1 pAXR1:AXR1* transgenic plants. As shown in Figure 2d, the expression levels of *AXR1* were significantly elevated in the *abt3-1 pAXR1:AXR1* plants. In consistent, these plants produced trichomes resembling those of WT plants (Figure 2b,c). Moreover, other developmental defects including wrinkled leave morphologies, shorter and less root hairs, and reduced plant stature and abnormal shoot architecture caused by the *ABT3* mutation were also restored in *abt3-1 pAXR1:AXR1* plants (Figure S4), suggesting that expression of *AXR1* is able to complement *abt3-1*. Collectively, these results indicate that *abt3-1* is defective in the *AXR1* gene, and *ABT3* is *AXR1*. We therefore renamed *abt3-1* as *axr1-32* according to the literatures (Martinez-Garda et al., 2020).

# AXR1 is localized to the nucleus of trichome cell

AXR1 has been reported to regulate several plant developmental processes including meristem function, tropic growth response, cell elongation as well as plant stature, leaf, fertility, and root hair development (Estelle & Somerville, 1987; Lincoln et al., 1990; Masucci & Schiefelbein, 1996), whether it also participates in trichome development regulation has not yet been reported. To explore the potential mechanism of AXR1 on trichome

136333x, 2023, 3, Downloaded from https://onlinelibrary.wiley.com/doi/10.1111/pj.16403 by Louisiana Sate University Lsu, Wiley Online Library on [12/12/2023]. See the Terms and Conditions (https://onlinelibrary.wiley.com/terms-and-conditions) on Wiley Online Library or rules of use; OA articles are governed by the applicable Creative Commons Licensea



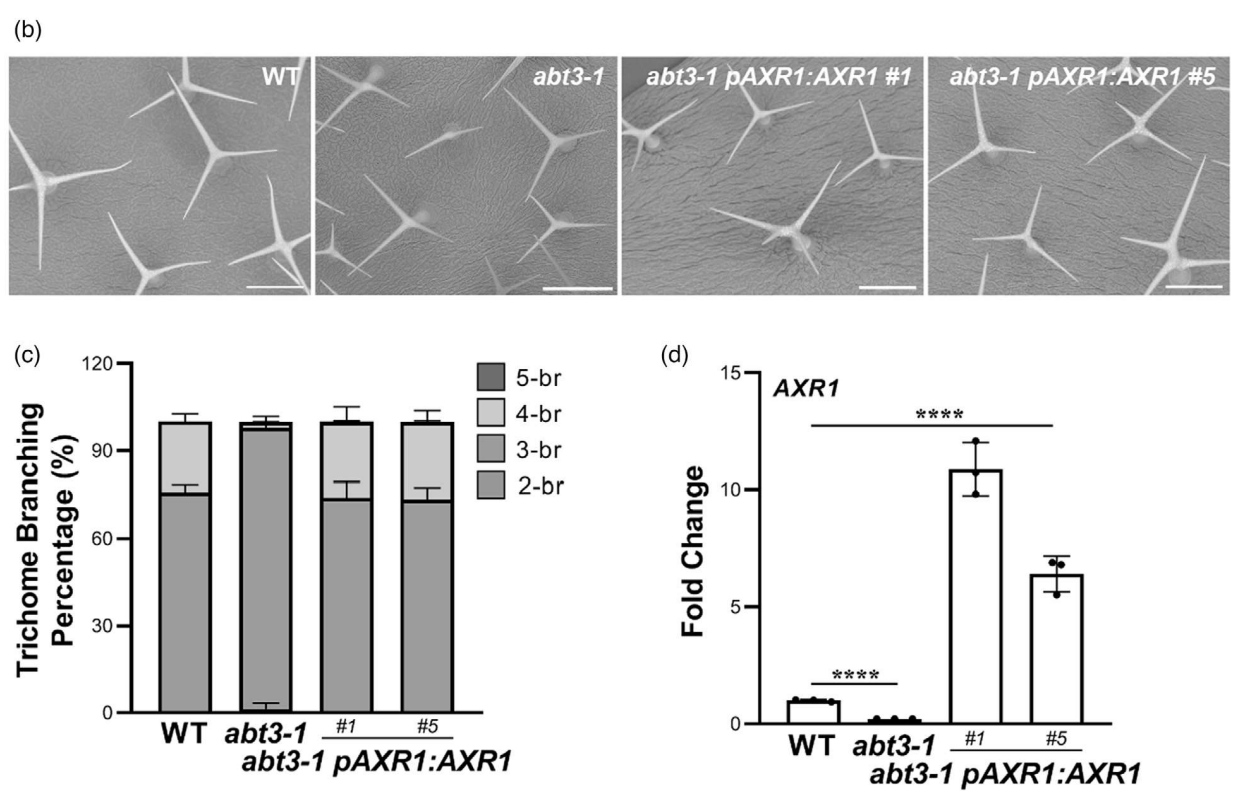


Figure 2. Genetic dissection of abt3-1 mutant.

(a) Map-base cloning of abt3-1. ABT3 locus was linked to molecular marker T25N20 on Chromosome I. Numbers of recombinants were shown under each marker. The asterisk indicates the position of AXR1 gene, AT1G05180. In the gene model, open boxes and solid lines represent the exons and introns, respectively. The 5'and 3'untranslated regions were shown as shaded boxes. The highlighted nucleotide below the gene model indicates the exact position of the mutation site.

(b) Trichome branching phenotypes of abt3-1 and the complementation lines. Scale bars = 250  $\mu$ m.

(c) Quantification analyses of trichome branch numbers on the third rosette leaves in plants shown in (b). 2/3/4/5-br for two/three/four/five-branched trichomes, respectively. Data were presented as mean  $\pm$  SD.

(d) RT-qPCR analysis of AXR1 transcripts levels in WT, abt3-1 and the complementation lines. Fold changes were calculated with respect to the expression levels in the WT. Student's t-test was used to assess the difference from WT (\*\*\*\*, P < 0.0001).

morphogenesis, we first examined the expression patterns of *AXR1* in trichomes by generating *pAXR1:AXR1-GFP* plants. The *pAXR1:AXR1-GFP* construct can restore the developmental impairments of *axr1-3* (Figure S5), indicating that AXR1-GFP is functional *in planta*. In contrast to that of *axr1* mutants (Figure S3e–f), the trichome branching was induced in *pAXR1:AXR1-GFP* plants accompanying the elevated *AXR1* expression levels (Figure 3a–c), indicating that *AXR1* is required for trichome morphogenesis. The localization of AXR1 in trichome cells was investigated by tracking the GFP fluorescence using confocal laser microscope. As shown in Figure 3d, clear GFP signals were observed in the nucleus of trichome cell, implying that *AXR1* might function in nuclei to regulate trichome development.

# AXR1 genetically interacts with ROP2 to regulate trichome branching

Since previous studies have showed that AXR1 is required for auxin signal transduction (Leyser, 2018) and auxin regulates pavement cell morphogenesis mainly through ROPs signaling (Chen et al., 2014; Kang et al., 2017; Li et al., 2017; Lin et al., 2013; Xu et al., 2010, 2014), we speculated whether the regulation of AXR1 on trichome shapes is also mediated by ROPs. For a first step, we examined trichome phenotypes of CA-ROP2 mutants, where the activities of ROP2 is constitutively activated (Li et al., 2001). As shown in Figure 4a,b, CA-ROP2 plants displayed similar trichome branching defects that was similar to those in axr1 mutants. In CA-ROP2 plants, four-branched trichomes disappeared on the 3rd rosette leaves, compared to that of about 25% in WT plants (Figure 4a,b). More strikingly, twobranched trichomes, which were absent in WT plants became pervasive in CA-ROP2 plants and whose proportion reached to  $\sim$ 26% (Figure 4a,b), suggesting the suppression of trichome branching induced by constitutively activation of ROP2. To confirm the effects of CA-ROP2 on trichome morphogenesis, we generated ROP2 overexpression plants (Figure 4c). Although not as striking as that in CA-ROP2 plants, the trichome branching in p35S:ROP2-GFP was inhibited as well. In p35S:ROP2-GFP plants, the percentage of three-branched trichomes was increased to  $\sim$  94% versus the  $\sim$ 75% in the WT, while the proportion of four-branched trichomes fell to  $\sim\!6\%$  compared to that of  $\sim\!25\%$  in the WT. Meanwhile, we also examined the trichome phenotypes of dominant negative ROP2 (DN-ROP2) plants in which the activities of ROP2 are repressed (Li et al., 2001). Although it is not very striking, 4-branched trichomes were mildly promoted ( $\sim\!28\%$  versus the  $\sim\!22\%$  in the WT). Moreover, a few ( $\sim\!0.6\%$ ) of 5-branched trichomes were observed in DN-ROP2. These observation indicating that downregulation of the ROP2 levels may potentially promote trichome branching. Interestingly, as that of AXR1, we found that ROP2 is also highly expressed in trichome nucleus (Figure 4d), implying ROP2 may regulate trichome morphogenesis through responding nuclear signals.

Given the highly similar reduced trichome branching phenotypes of axr1 loss-of-function mutants and ROP2 overexpression plants and trichome nuclear localization of AXR1 and ROP2, we assumed AXR1 and ROP2 may be functionally related in regulating trichome morphogenesis. To this end, we introduced axr1-32 to CA-ROP2 background by crossing and examined the trichome phenotypes. As expected, in axr1-32 CA-ROP2 double mutants, the trichome branches numbers were further reduced compared to either of the axr1-32 or CA-ROP2 single mutants (Figure 5a,b). The proportion of two-branched trichomes rise to  $\sim$  78%, versus  $\sim$  1.5% and  $\sim$  24% in axr1-32 and CA-ROP2 mutants, respectively (Figure 5b). The proportion of three-branched trichomes dropped to  $\sim$  22%, and 4branched trichomes totally disappeared (Figure 5b). We also constructed axr1-3 CA-ROP2 plants, which showed similar trichome branching phenotypes as those in axr1-32 CA-ROP2 (Figure 5a,c). Collectively, these results demonstrate that functional loss of AXR1 could enhance the severity of trichome branching defects in CA-ROP2, and AXR1 may genetically interact with ROP2 to regulate trichome development.

To validate the genetic relationship between *AXR1* and *ROP2* in regulating trichome branching, we further constructed *p35S:AXR1-GFP CA-ROP2* plants. As that control by its native promoter, constitutively expression of *AXR1* under control of the *CaMV 35S* promoter could also induce trichome branching (Figure 6a–c). In the strong *p35S:AXR1-GFP* line, a number of 5-branched trichomes



1365313x, 2023, 3, Downloaded from https://onlinelibrary.wiley.com/doi/10.1111/tpj.16403 by Louisiana State University Lsu, Wiley Online Library on [12/12/2023]. See the Terms and Conditions (https://onlinelibrary.wiley.com/terms-and-conditions) on Wiley Online Library for rules of use; OA articles are governed by the applicable Creative Commons Licenses

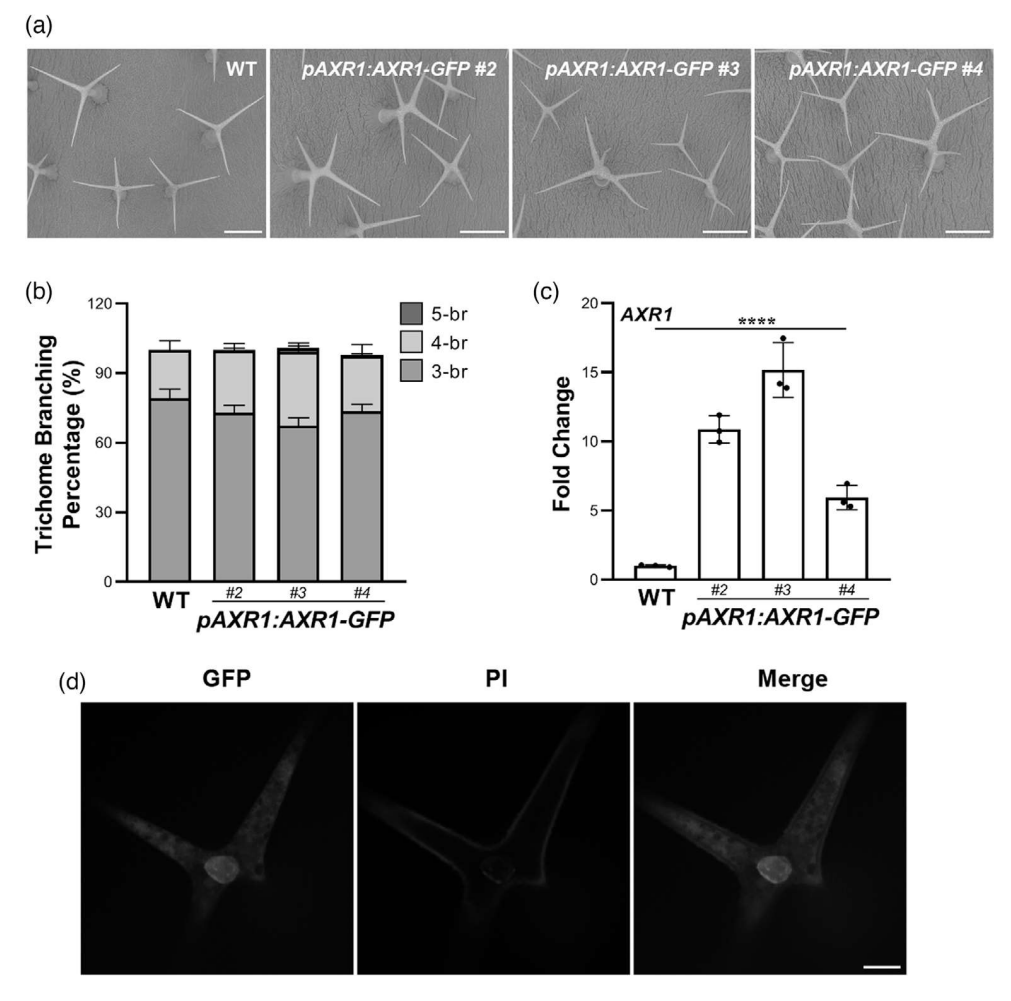


Figure 3. Investigation of AXR1 expressions in trichomes.

- (a) Representive trichomes on the fifth rosette leaves of WT and pAXR1:AXR1-GFP lines. Scale bars = 250 µm. #2/#3/#4 for independent transgenic lines, respectively
- (b) Quantification of trichome branching phenotypes of the plants shown in (a). 3/4/5-br for three/four/five-branched trichomes, respectively. Data were presented as mean  $\pm$  SD.
- (c) Examination of AXR1 transcripts levels in WT and pAXR1:AXR1-GFP lines by RT-qPCR. Fold changes were calculated with respect to the expression levels in the WT. Student's *t*-test was used to assess the difference from WT (\*\*\*\*, *P* < 0.0001).
- (d) Expression patterns of AXR1 in trichomes. pAXR1:AXR1-GFP plants were grown on MS for 10 days, and the first pairs of leaves were stained with DAPI solution (100 ng/ml) to indicate the nuclei. The blue fluorescence and green fluorescence were observed with the confocal microscope under the exciting light at 364 nm and 488 nm, respectively. The emission light were at 454 nm and 507 nm for DAPI and GFP, respectively. Images were acquired using the IQ3.0 imaging workstation software (Andor). Scale bar = 20  $\mu$ m.

( $\sim$ 2%) appeared on the third leaves (Figure 6a–c). When we crossed the weak p35S:AXR1-GFP line (#33) with CA-ROP2 plants, the proportion of two-branched trichomes significantly declined in p35S:AXR1-GFP CA-ROP2 plants compared to those in CA-ROP2 plants (Figure 6d,e), suggesting that overexpression of AXR1 is able to rescue the trichome branching reduction in CA-ROP2. Because in p35S:AXR1-GFP CA-ROP2 plants, the expression of AXR1 and ROP2 were both under control of the CaMV 35S promoter, to exclude whether the trichome phenotypes in p35S:AXR1-GFP CA-ROP2 was caused by co-suppression, we examined the expression levels of AXR1 and ROP2 in

p35S:AXR1-GFP CA-ROP2, respectively. As shown in Figure 6f, although not as remarkable as that in the corresponding overexpression plants, AXR1 and ROP2 transcripts were still apparently accumulated in p35S:AXR1-GFP CA-ROP2 plants compared to those in WT, implying that the trichome phenotypes in p35S:AXR1-GFP CA-ROP2 is due to the fluctuation of AXR1 and ROP2 expression levels. We also generated axr1-3 rop2 rop4i mutants by crossing and whose trichome phenotypes were investigated. As shown in Figure S7a,b, the trichome branching phenotypes resemble that of the rop2 rop4i mutants, suggesting that repression of ROP2 and ROP4 is able to

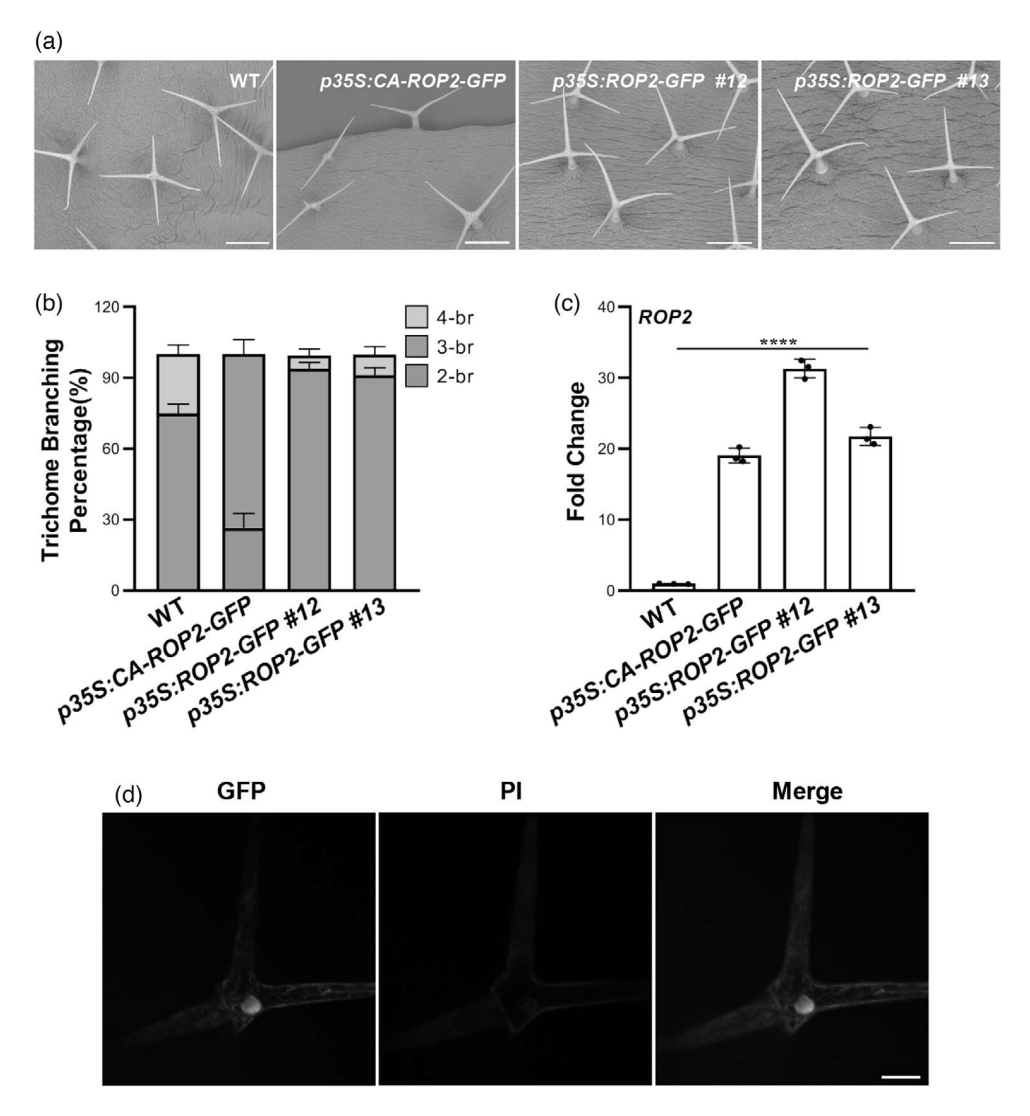


Figure 4. Analyses of ROP2 function on trichome development.

(a) Trichome branching phenotypes of WT, p35S:CA-ROP2-GFP (CA-ROP2), and p35S:ROP2-GFP plants. #12/#13 for independent transgenic lines, respectively. Scale bars = 250  $\mu$ m.

(b) Proportion of different branched trichomes on the third rosette leaves of the plants shown in (a). 2/3/4-br for two/three/four -branched trichomes, respectively. Data were presented as mean  $\pm$  SD.

(c) RT-qPCR analyses of ROP2 transcripts levels in WT, CA-ROP2 and p35S:ROP2-GFP plants. Fold changes were calculated with respect to the expression levels in the WT, Student's t-test was used to assess the difference from WT (\*\*\*\*, P < 0,0001),

(d) Examination of localization of ROP2 in trichome. The procedures were the same as that described in Figure 3d. Scale bar =  $20 \mu m$ .

suppress *axr1* mutant phenotype. Taken together, we conclude *AXR1* genetically interacts with *ROP2*, and *AXR1* may modulate trichome morphogenesis through negatively regulating *ROP2*.

# AXR1 mediates ROP2 degradation

To further clarify the regulatory mechanism of *AXR1* on *ROP2* during trichome morphogenesis, we examined the expression levels of *ROP2* in *axr1* mutants. However, we did not find significant differences among the WT and *axr1* mutants (Figure 7a), suggesting that the regulation of

AXR1 on ROP2 may be beyond transcriptional level. Previous studies have showed that besides regulating the degradation of proteins functioning in auxin signaling, AXR1 also mediates the degradation of other proteins such as cell cycle regulator KRP1 and E2FC, cytokinin signaling component ARR5, and transcription factors HY5 and HYH (del Pozo, Boniotti, et al., 2002; del Pozo, Dharmasiri, et al., 2002; Li et al., 2013; Ren et al., 2008; Schwechheimer et al., 2002). Based on the genetic analyses and the instability characteristics of ROP2 protein reported before (Chai et al., 2016), we hypothesized the involvement of AXR1 on

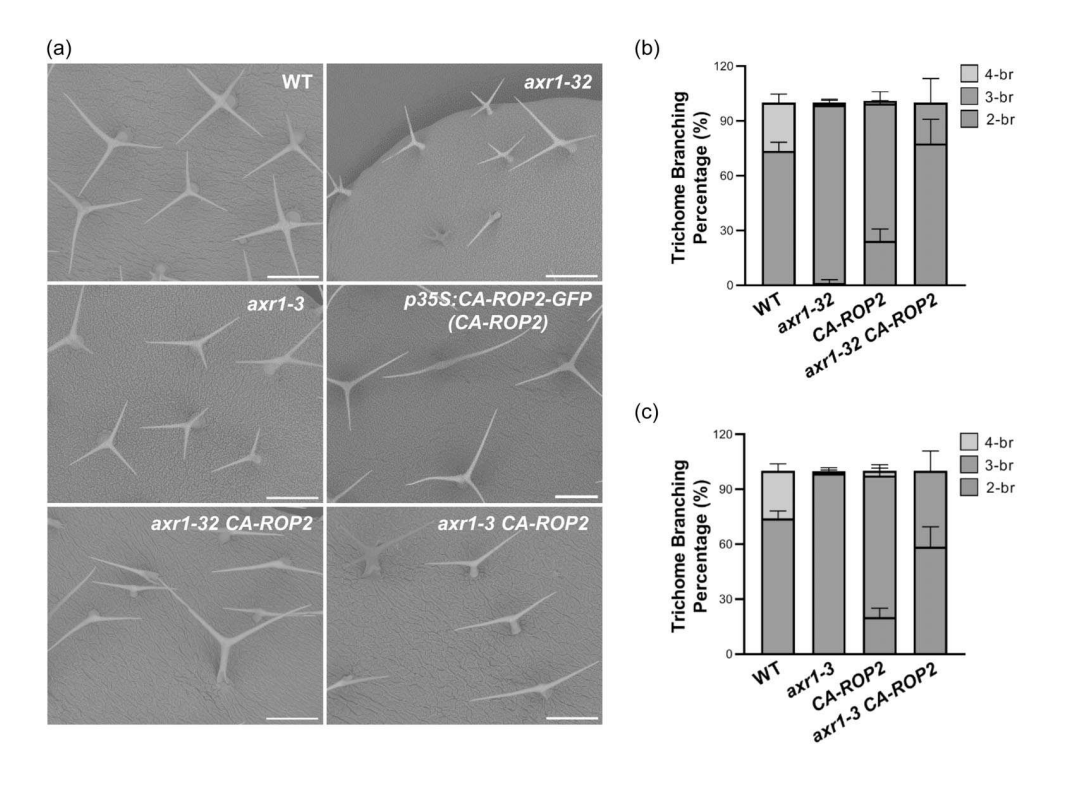


Figure 5. The AXR1 mutation enhances trichome phenotypes of CA-ROP2. (a) Representive trichomes on the fifth rosette leaves of WT, axr1-32, axr1-3, CA-ROP2, axr1-32 CA-ROP2 and axr1-3 CA-ROP2. Scale bars = 250 µm. (b,c) Quantification of trichome branching phenotypes on the third rosette leaves of axr1-32 CA-ROP2 plants (b) and axr1-3 CA-ROP2 plants (c). 2/3/4-br for two/ three/four-branched trichomes, respectively. Data were presented as mean  $\pm$  SD.

ROP2 degradation. To this end, we examined the total protein abundance of ROP2 in axr1 mutants using anti-ROP2 antibody. In axr1-32 mutants, the steady-state ROP2 levels were remarkably accumulated (about 2.3 fold compared to those in WT plants, Figure 7b,c). The similar results were obtained in axr1-3 background (about 2.0 fold compared to those in WT, Figure 7b,c), suggesting that functional loss of AXR1 results in the accumulation of ROP2 and the regulation of *ROP2* by *AXR1* is likely at the protein level.

To further illustrate the regulation of AXR1 on ROP2 protein fluctuation, we investigated ROP2 stability in the extracts prepared from WT and axr1-32 mutant respectively through an in vitro cell-free degradation assay (Wang

et al., 2009). As shown in Figure 7d,e, we confirmed that ROP2 is an unstable protein and is degraded through the 26S proteasome as described by Chai et al. (2016). In WT cell extracts, the amount of in vitro added His-ROP2 combined protein decreased during the time lapse without the proteasome inhibitor MG132 (Figure 7d). Quantification of the degradation of kinetics showed that the half-life  $(t_{1/2})$ was about 6.8 h (Figure 7e). When MG132 was added, degradation of the His-ROP2 was significantly delayed and the half-life  $(t_{1/2})$  was remarkably prolonged (Figure 7d,e). However, when we examined the degradation of His-ROP2 in cell extracts from axr1-32 mutant using the similar approach, the abundance of His-ROP2 was significantly

Figure 6. Overexpression of AXR1 suppresses CA-ROP2 trichome branching phenotypes.

<sup>(</sup>a) Trichome branching phenotypes of AXR1 overexpression lines, #18/#33/#34 for independent transgenic lines, respectively. Scale bars = 250 µm.

<sup>(</sup>b) Quantification trichome branch numbers of the plants shown in (a), 3/4/5-br for three/four/five-branched trichomes, respectively. Data were presented as mean  $\pm$  SD.

<sup>(</sup>c) Expression levels of AXR1 in the overexpression plants. Fold changes were calculated with respect to the expression levels in the WT. Student's t-test was used to assess the difference from WT (\*\*\*\*, P < 0.0001).

<sup>(</sup>d) Trichome branching phenotypes of p35S:AXR1-GFP CA-ROP2 plants. Scale bars = 250  $\mu$ m.

<sup>(</sup>e) Quantification of trichome branch numbers of p35S:AXR1-GFP CA-ROP2 plants. 2/3/4-br for two/three/four-branched trichomes, respectively. Data were presented as mean  $\pm$  SD.

<sup>(</sup>f) Expression levels of AXR1 and ROP2 in different genetic backgrounds, Fold changes were calculated with respect to the expression levels in the WT. Student's t-test was used to assess the difference from WT (n.s. not significant, \*, P < 0.1, \*\*\*\*, P < 0.0001).

136333x, 2023, 3, Downloaded from https://onlinelibrary.wiley.com/doi/10.1111/tpj.16403 by Louisiana State University Lsu, Wiley Online Library on [12/12/2023]. See the Terms and Conditions (https://onlinelibrary.wiley.com/terms-and-conditions) on Wiley Online Library for rules of use; OA articles are governed by the applicable Creative Commons. License and Conditions (https://onlinelibrary.wiley.com/terms-and-conditions) on Wiley Online Library for rules of use; OA articles are governed by the applicable Creative Commons. License are the applicable Creat



136333x, 2023, 3, Downloaded from https://onlinelibrary.wiley.com/doi/10.1111/tpj.16403 by Louisiana State University Lsu, Wiley Online Library on [12/12/2023]. See the Terms and Conditions (https://onlinelibrary.wiley.com/terms-and-conditions) on Wiley Online Library for rules of use; OA articles are governed by the applicable Creative Commons. License and Conditions (https://onlinelibrary.wiley.com/terms-and-conditions) on Wiley Online Library for rules of use; OA articles are governed by the applicable Creative Commons. License are the applicable Creat

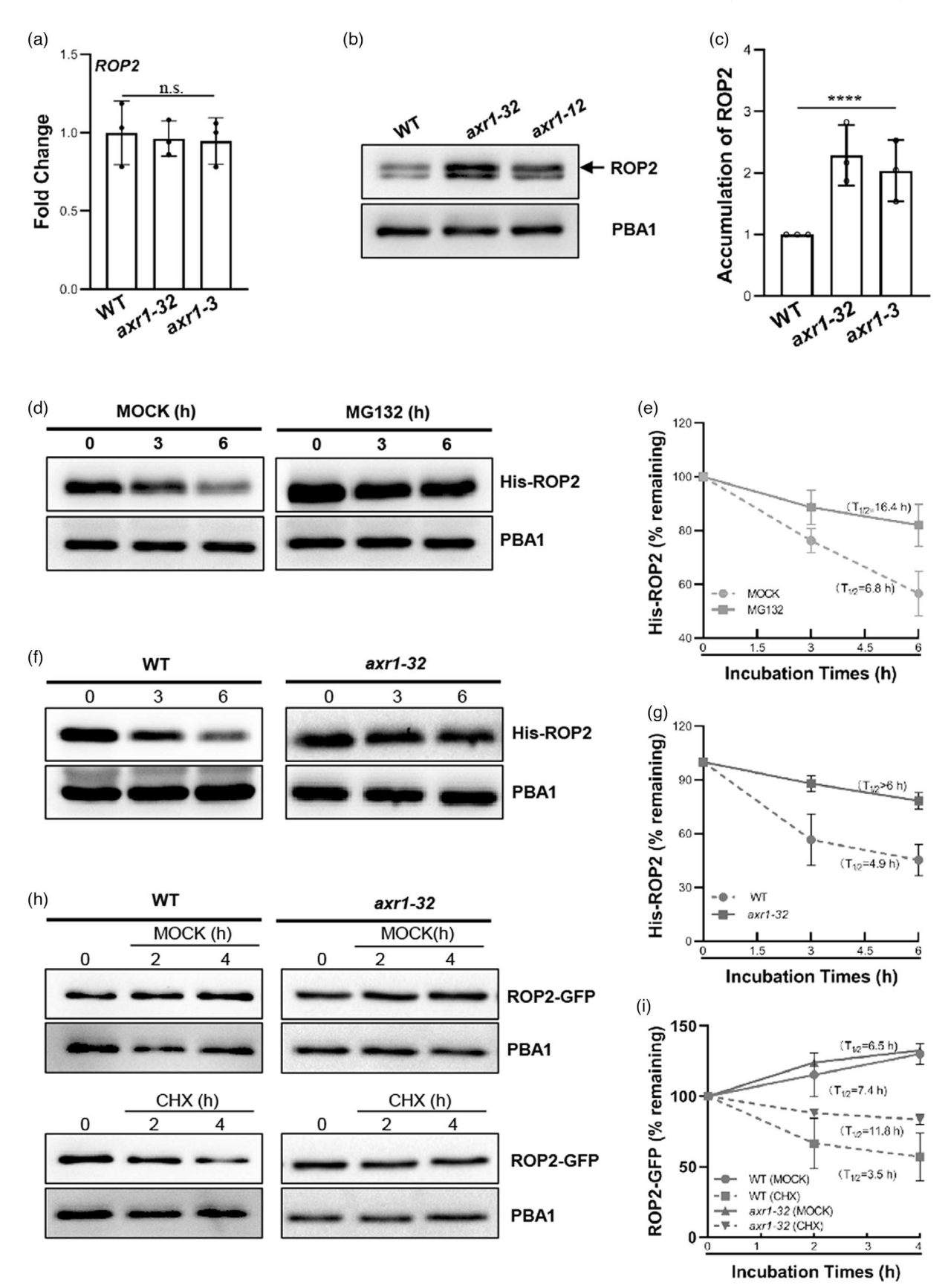


Figure 7. AXR1 mediates proteasome dependent ROP2 degradation.

(a) Examination of expression levels of *ROP2* transcripts in *axr1* mutants by RT-qPCR. Fold changes were calculated with respect to the expression levels in the WT. Student's t-test was used to assess the difference from WT (n.s. not significant).

(b) Investigation of steady-state ROP2 levels in axr1 mutants through immuno-blotting with anti-ROP2 antibody. The amount of PBA1 was used as the loading control.

(c) Quantification of steady-state ROP2 levels in axr1 mutants detected in (b). Data were presented as mean  $\pm$  SD of three biological replicates. Student's t-test was used to assess the difference from WT (\*\*\*\*, P < 0.0001).

(d) In vitro cell-free degradation assay of His tagged ROP2 in WT background. Total proteins were extracted from WT and purified His-ROP2 proteins were added and incubated with or without MG132 at the indicated times. The steady-state His-ROP2 were detected by western blotting with anti-His antibody. The amount of PBA1 was used as the loading control.

(e) Statistic analyses of the His-ROP2 levels shown in (d). The half-life time was predicted based on the regression equation.

(f) In vitro cell-free degradation assay of His tagged ROP2 in axr1-32 background. The purified His-ROP2 proteins were added to the total proteins extracted from WT and axr1-32, respectively, and incubated at the indicated times. The steady-state His-ROP2 were detected by western blotting with anti-His antibody. The amount of PBA1 was used as the loading control.

(g) Statistic analyses of the His-ROP2 levels shown in (f). The half-life time was predicted based on the regression equation,

(h) Protoplast-based protein degradation assay of ROP2-GFP proteins in WT and axr1-32. Mesophyll protoplasts prepared from WT and axr1-32 plants were transfected with p35S:ROP2-GFP transient expression plasmids for 12 h, and then treated with CHX over the indicated time course, respectively. After that, total protein were extracted and ROP2-GFP were examined with anti-GFP antibody. The amount of PBA1 was used as the loading control.

(i) Statistic analyses of the ROP2-GFP levels shown in (h). The half-life time was predicted based on the regression equation.

retained compared that in WT (Figure 7f,g). After 6 h incubation, the His-ROP2 in the cell extracts from WT was almost exhausted, while in the *axr1-32* background, about 78% His-ROP2 protein could still be detected on the gel (Figure 7f,g), suggesting the stabilization of ROP2 in *axr1-32* mutant.

To confirm the modulation of AXR1 on ROP2 stability, we performed mesophyll protoplast-based degradation assay (Wang et al., 2009). Transiently expression vector p35S:ROP2-GFP were transformed into the mesophyll protoplasts from WT and axr1-32 mutant, respectively, and the ROP2-GFP abundance were examined during the time course. As shown in Figure 7h,i, we found although relative higher in axr1-32 within 2 h, the amount of ROP2-GFP was comparable between WT and axr1-32 mutant without the cytosolic translation inhibitor cycloheximide (CHX) (Figure 7h,i). However, when CHX was presented, the amount of the ROP2-GFP significantly dropped after 4 h incubation in WT protoplasts (only about 48% of the original amount left, Figure 7h,i), suggesting the degradation of ROP2-GFP. When CHX and MG132 were simultaneously added during the incubation, the degradation of the ROP2-GFP could be inhibited (Figure S8). In contrast to that in WT, after 4 h incubation with CHX, abundant steady-state ROP2-GFP protein could be detected in axr1-32 protoplasts (about 84% of the original amount left, Figure 7h,i), suggesting AXR1 mutation delayed ROP2 degradation. These results are consistent with the in vitro analysis described above. Taken together, we conclude AXR1 mediates ROP2 stability, and functional loss of AXR1 could lead to the accumulation of steady-state ROP2.

# **DISCUSSION**

# AXR1 is required for trichome development in Arabidopsis

In our long-term attempts to identify new components in the genetic network that participate in trichome

development, a trichome branching defective mutant, *abt3-1*, was isolated through the genetic screens (Figure 1c–e). Molecular cloning and genetic complementation analyses confirmed that *ABT3* is identical to the locus *AXR1* (Figure 2; Figure S2, S4), and *abt3-1* represents a novel allele of *AXR1*, *axr1-32*.

AXR1 has been characterized to be indispensable for a range of auxin mediated plant developmental processes including plant size and stature, apical dominance, fertility, leaves, root gravitropism, hypocotyl elongation and root hair development (Estelle & Somerville, 1987; Lincoln et al., 1990; Masucci & Schiefelbein, 1996). However, whether AXR1 is required for trichome development remains unclear. Take advantage of the isolation of axr1-32 mutant, we revealed the regulation of AXR1 on trichome development. Functional loss of AXR1 lead to reduction of trichome branch numbers remarkably (Figure 1c–e), and strong AXR1 overexpression plants promote trichome branching (Figure 6a–c), suggesting that AXR1 functions as a positive regulator during trichome branching.

Given the fact that AXR1 servers as a pivotal component during auxin signaling transduction (Leyser, 2018), whether the regulation of AXR1 on trichome development is also mediated by auxin signaling is worthy of consideration. Interestingly, our preliminary studies implied that auxin and AXR1 seems to be discriminatory required for trichome development, because we found increase of endogenous auxin levels by overexpression of auxin biosynthesis gene YUCCA2 (YUC2) gene under control of CaMV 35S promoter or MERISTEM LAYER L1 (ML1) all led to the decrease of trichome branch numbers (Figure S9). The proportion of three-branched trichomes was apparently increased (  $\sim$  92% in pML1:YUC2 and  $\sim$  92% in p35S:YUC2 compared to that of  $\sim$ 78% in the WT). Moreover, a few two-branched trichomes were also observed in pML1:YUC2 ( $\sim$ 0.7%) and p35S:YUC2 ( $\sim 2.7\%$ ) plants, respectively. To validate the effects of auxin signal on trichome development, we also

characterized the trichome branching phenotypes of a homozygous T-DNA insertion mutant allele of TRI1 (tir1-10) (Wang et al., 2020). Only a mild decrease of trichome branch numbers were observed in tir1-10 mutant (Figure S9c,d), which is in contrast to that of axr1 plants. These contrary results complicated the effects of auxin on trichome development, and one possible explanation may be due to the dosage-dependent effects. The formation of proper trichome branches may require precise auxin levels and excessive auxin possibly inhibits trichome branching. Alternatively, the regulation on trichome development may represent a unique and specific function of AXR1, which is independent of auxin signaling pathway.

The cell cycle is also closely associated with trichome branching. The developing trichome typically undergoes endorepduplication instead of mitosis and eventually makes the nuclear DNA reach to 32C (C equals haploid DNA content per nucleus), accompanied by the formation of three to four branches (Schnittger & Hülskamp, 2002). Generally, mutations in genes that increase or decrease the levels of endoreduplication elevate or educe the trichome nuclei size and branch numbers, respectively (Ishida et al., 2008; Tominaga-Wada et al., 2011). To investigate whether the decrease of trichome branch numbers in axr1 is linked with altered endoreduplication levels, we examined the trichome nuclei size of axr1-32 as well as axr1-3 by DAPI staining. Smaller nuclei and decreased nuclei size were observed in the mature trichome of axr1 mutants compared with those of the WT (Figure S10), indicating the regulation of AXR1 on trichome branching may also involve in the cell cycle control. This is reasonable because AXR1 was reported to promote the proteolysis of cell cycle regulator KRP1 and overexpression of which leads to the production of trichomes with reduced branch numbers (Ren et al., 2008; Schnittger et al., 2003).

# ROP2 participates in both trichome branching extension and trichome initiation

The best known functions of ROPs are in the context of orchestrating epidermal cell morphologies (Liu et al., 2021; Ou & Yi, 2022); however, whether ROPs also involve in trichome development remains unclear. Fu et al. (2002) reported that CA-ROP2 expression causes mild distorted trichome phenotypes, while the number of branches is not affected. Under our growth condition, we also observed the abnormity of the branch morphologies in CA-ROP2 plants. A proportion of CA-ROP2 mutant trichomes display three branches but one of them is extremely short or only have a protrusion (Figure 4a), suggesting the repression of branch extension. The branch site initiation seems also impaired due to CA-ROP2 expression, since the first two branches are much farther apart compared with those in WT (Figure 4a), which is consistent with the observations reported by Fu et al. (2002). However, besides the branch

morphologies, we found the branch numbers are significantly reduced in CA-ROP2 trichomes (Figure 4a). Twobranched trichomes which are rare in WT become popular in CA-ROP2 (Figure 4a,b). In contrast, four-branched trichome almost extinct comparing of about 25% in WT (Figure 4a,b). Accordingly, although not as striking as that in CA-ROP2 plants, overexpression of ROP2 also resulted in a certain degree of decrease of trichome branching numbers (Figure 4a,b), suggesting the negative regulation of ROP2 on trichome branching. Notably, the amount of ROP2 transcripts is higher in p35S:ROP2-GFP #12 than that in CA-ROP2 (Figure 4c), indicating that besides the transcripts levels, the regulation of ROP2 on trichome branching also depend on ROP2 activities. Together, these results provide evidences for the involvement of ROP2 in the regulation of trichome morphogenesis, further expanding our understanding of ROP2's roles in modulating epidermal cell development in plants.

In addition, ROP2 modulates cell expansion largely depending on its regulation on cytoskeleton organization (Fu et al., 2002, 2005; Kang et al., 2017; Li et al., 2017), whether ROP2 is similarly associated to trichome morphogenesis remains unknown. Given the striking effects of microtubule cytoskeleton dynamics on trichome branch initiation (Ishida et al., 2008; Mathru & Chua, 2000; Tominaga-Wada et al., 2011), we examined the configuration of cortical microtubule in CA-ROP2 trichomes by crossing CS6550, the TUB6-GFP fluorescent marker line, with CA-ROP2 but no apparent abnormity were observed compared to those in WT (Figure S11b). We also conducted drug treatment with oryzalin, which disrupts microtubule assembly (Mathru & Chua, 2000). Most of the CS6550 trichomes were two-branched with swollen morunder continuous orvzalin phology treatment (Figure S11a). In contrast, the shape changes of CA-ROP2 trichomes were grosser, since the majority of the trichomes displayed almost ballooned shapes without discriminable branches (Figure S11a). Further analyses of the cortical microtubule organization found short and crossed microtubules in WT trichomes and microtubule meshes in CA-ROP2 trichomes instead of longitudinal microtubule cables in untreated trichomes (Figure S11b). These observations indicate that CA-ROP2 trichomes are more sensitive to oryzalin treatment, and ROP2 might also facilitate cytoskeleton dependent trichome morphogenesis.

# AXR1 interacts with ROP2 to controls trichome cell shape

The spatiotemporal activity of ROPs are regulated by a range of factors during epidermal cell morphogenesis (Chai et al., 2016; Igisch et al., 2022; Lin et al., 2015; Liu et al., 2021). Auxin was characterized as the upstream positive signal to regulate ROP2 activities during pavement cell interdigitation, and trace of exogenous auxin could rapidly activate ROP2 (Xu et al., 2010, 2014). However, based on

phenotypic examination and biochemical investigation, we found that AXR1 negatively regulates ROP2 during trichome branching. Functional loss of AXR1 could enhance the trichome phenotypes of CA-ROP2 and lead to the accumulation of steady-state of ROP2 levels (Figures 5 and 7). Meanwhile, overexpression of AXR1 could alleviate the trichome branching defects induced by constitutive activation of ROP2 (Figure 6). These inconsistent results may be due to the fact that the general function of AXR1 is in protein proteolysis rather than in auxin response per se. First, axr1 mutants also display resistance to other hormones. axr1-3 allele is more resistant to inhibition of root growth induced by MeJA treatment and AXR1 promotes the cytokinin response by facilitating ARR5 proteolysis (Li et al., 2013; Tiryaki & Staswick, 2002). Second, AXR1 is required for different pathways that are controlled by E3-mediated protein degradation. Cell cycle regulator E2FC and KRP1 are degraded by the ubiquitin-SCFSKP2 pathway, which depends on AXR1 mediated RUB conjugation (del Pozo, Boniotti, et al, 2002; del Pozo, Dharmasiri, et al., 2002; Ren et al., 2008). AXR1 is also involved in the COP1/COP10/ CSN-mediated repression of photomorphogenesis in the dark through mediating HY5 and HYH degradation (Schwechheimer et al., 2002). Therefore, we hypothesize that the involvement of AXR1 and ROP2 interaction in trichome morphogenesis may mainly depend on the proteolytic function of AXR1 and represent a new regulator pathway on ROP2 activity.

In addition, we found both of AXR1 and ROP2 highly expressed in trichomes nuclei (Figures 3d and 4d), suggesting AXR1 and ROP2 possibly interact in the nuclei to regulate trichome development. During pavement cell interdigitation and root hair development, ROP2 was localized preferentially to the cortical region of the cell to promote expansion (Chai et al., 2016; Fu et al., 2002, 2005). These observations emphasize that the manipulation of ROP2 on different cellular and developmental processes may through different mechanisms. Despite we failed to establish the direct interaction and the cellular compartments where they interact, these findings revealed a new factor and a distinct pathway that involves in regulation ROP2, further enriching our understanding of the function of ROP2 on cell morphogenesis.

# **EXPERIMENTAL PROCEDURES**

# Plant material and growth condition

All the plant materials used in this study are in *Columbia-0 (Col-0)* ecotype background unless indicated otherwise. Wild type (WT) refers to Col-0 plants. *CA-ROP2, DN-ROP2,* and *rop2rop4i* plants were kindly provided by Prof. Lin (Fujian A&F University). The *abt3-1 (axr1-32)* mutant was isolated from a *gl2-3 (Salk\_039825,* Wang et al., 2010) ethyl methanesulfonate (EMS)-mutagenesis population we established before. The *axr1-3 (CS3075), tir1-10 (Salk\_090445,* Wang et al., 2020), and *CS6550* mutants were

obtained from the Arabidopsis Biological Resources Center (ABRC). pAXR1:AXR1, pAXR1:AXR1-GFP, p35S:AXR1-GFP, and p35S:ROP2-GFP transgenic lines were produced by the Agrobacterium tumefaciens-mediated floral dip plant transformation method (Clough & Bent, 1998). The transgenic plants were obtained through antibiotic-resistant selection, genomic PCR confirmation, and T3 plants were used for phenotype measurements and other experiments. Primers used in the construction of the corresponding plasmids are listed in the Table S1. abt3-1 (axr1-32) CA-ROP2, axr1-3 CA-ROP2, and p35S:AXR1-GFP CA-ROP2 plants were constructed by crossing the corresponding single mutants and the double mutants were identified by the GFP fluorescence examination and genomic PCR genotyping in the F2 population. The confirmed plants were used for trichome branching phenotype characterization.

For plant culture, the seeds were stratified at 4°C for 2 days and then sowed on commercial soil mix (Pindstrup) for germination and growth in a growth room at  $22\pm1^{\circ}C$  under continuous illumination ( $\sim100~\mu\text{mol}~\text{m}^{-2}~\text{sec}^{-1}$ ). For protoplast preparation, seeds were sowed and grown on Jiffy-7-Peat Pellets (Jiffy Group, Zwijndrecht, Netherlands) in a growth chamber (Conviron A1000, British Columbia, Canada) with day/night cycle (12 h/12 h) at  $22\pm1^{\circ}C$ , and fully expanded rosette leaves of 30 days old plants were used.

# Trichome phenotypic characterization

Trichome branching phenotypes were examined as described by Liang et al. (2019). In short, plants in different genotype backgrounds were grown in soil for 3 weeks and the representive trichomes on the 5th or 6th rosette leaves were imaged by using scanning electron microscopy (SEM TM3030, Hitachi, Japan). Meanwhile, the branch numbers of trichomes on the 3rd and 4th rosette leaves were counted and recorded. For each genotype plant, at least 15 individuals were used for quantitative analysis, and all experiments were repeated at least three times. Student's t-test was used to assess the difference.

#### Map-based cloning

Map-based cloning was conducted according to Lukowitz et al. (2000). First, abt3-1 mutant was crossed with Arabidopsis Landsberg erecta (Ler) ecotype and F2 segregation population was generated. Second, bulk segregant analysis (BSA) with 25 pairs molecular markers which cover all five Arabidopsis chromosomes was employed to roughly locate the mutation site in abt3-1. Third, fine mapping with additional molecular markers were carried out to narrow down the physical interval harboring the mutation site. Last, candidate genes in the final interval were sequenced to determine the mutation site. Sequence information of the molecular markers used was listed in the Table S1.

# RNA extraction and real-time quantitative PCR (RT-qPCR)

Total RNAs were extracted from the latest emerging rosette leaves of 2-week-old soil grown plants in different genotype background with TRIzol reagent (15596–026, Invitrogen, Waltham, MA, USA). Reverse transcriptions were carried out by using the Uelris RT mix with DNase (All-in-one) (R2020, US Everbright® Inc, America) with 1  $\mu g$  total RNAs and oligo (dT15) primers. Quantitative real-time PCR (qPCR) was performed with the FastStart Essential DNA Green Master kit (06402712001, Roche, Basel, Switzerland) and Bio-Rad CFX96 real-time PCR system. Relative expression levels of the target genes were calculated with  $2^{-aCt}$ . Expressions of ACTIN2 (ACT2) was used as the internal controls. Primers for qPCRs were listed in Table S1.

# Spinning-disk confocal microscopy imaging

The localization of AXR1 and ROP2, and cMTs configuration in trichome cells were investigated with a spinning-disk confocal system consists of a DMi8 inverted microscope (Leica, Wetzlar, Germany), a CSU-W1 confocal scanner unit (Yokogawa, Tokyo, Japan), and an iXon Ultra 888 EMCCD camera (Andor, England). GFP were excited at 488 nm. Fluorescent dye 4',6-diamidino-2phenylindole (DAPI) was excited at 364 nm. The emission wavelength of GFP and DAPI were 507 nm and 454 nm, respectively. Digital images were acquired with the IQ3.0 Imaging Workstation software (Andor, England).

The fluorescent signals of AXR1-GFP, ROP2-GFP, and cMTs were observed with a HC PL APO 40x objective. Because of the three-dimension geometry characteristics of the trichomes, z-stack imaging was employed with a 1  $\mu$ m z-step.

# Protein expression and purification

For expression and purification of the recombined His-ROP2 protein, the coding region of ROP2 was cloned into pET28a vector to generate pET28a-ROP2 recombine plasmid. After sequencing, the confirmed plasmid was transformed into Escherichia coli Rosetta (DE3) strain. The combined His-ROP2 protein was induced to express with 0.1 mm isopropylb-D-thiogalactopyranoside (IPTG) over night at 16°C and purified through Ni2+ beads (17-5318-02, GE, America) according to the manufacturer's instructions.

# Protein degradation assay

The protein degradation assay were conducted according to Wang et al. (2009). For in vitro experiments, about 3 g leaf tissues of 15d-old soil grown plants in different genetic backgrounds were harvested and grounded in liquid nitrogen. Total proteins were extracted with 3 ml degradation buffer (25 mm Tris pH 7.5, 10 mm NaCl, 10 mm MgCl<sub>2</sub>, 4 mm PMSF, 5 mm DTT, 10 mm ATP) for 40 min on ice. The concentrations of total proteins were determined by the Bio-Rad protein assay and were adjusted to be equally with the degradation buffer. After that, 500 ng His-ROP2 recombinant protein was added and incubated at 22°C for indicated times. At each time interval, 20 µl of the reaction products were taken and boiled in the same volume SDS sample buffer for 10 min to stop the reaction. The abundance of His-ROP2 was determined by western blotting with anti-His antibody (ab18184, Abcam, Cambridge, UK).

For protoplast based protein degradation assay, the transient expression plasmid p35S:ROP2-GFP was constructed and transformed to the WT and axr1-32 mesophyll protoplasts respectively according to Yoo et al. (2007). 20 µg plasmids were transformed into 200 µl protoplast cells and expressed at dark for 10-12 h in W5 buffer (154 mм NaCl, 125 mм CaCl<sub>2</sub>, 5 mм KCl, 2 mм MES). The transfected cells were then treated with 50  $\mu m$  cycloheximide (CHX) or the same volume DMSO for the indicated times. The reaction products at each time intervals were centrifuged and the pellets were quickly froze in liquid nitrogen to extract the total proteins. Protein levels of ROP2-GFP were analyzed by western blotting with anti-GFP antibodies (ab290, Abcam).

To examine the accumulation of endogenous ROP2, the latest emerging rosette leaves of 2-week-old soil grown plants were harvested. Total proteins were extracted with degradation buffer and ROP2 levels were estimated by western blotting with anti ROP2 antibody (R2165-2, Abiocode; Ren et al., 2016).

For all the immune blotting assay, the anti-PBA1 (ab98861, Abcam, England) was used to indicate the loading amount.

# Trichome nuclei size measurements

The experiments were conducted according to Szymanski and Marks (1998). Trichomes on in the 3rd rosette leaves of 3-week-old soil grown WT and axr1 mutants were used for analyses. Leaves from different genotypes were collected and fixed with MgCl2 solution (3:1(v/v) mixture of 95% ethanol and glacial acetic acid, 1 mm MgCl<sub>2</sub>), respectively. Cell nuclei were stained with DAPI (100 ng/ml) and viewed under the fluorescence microscope (DM 5000B, Lecia) and images were captured. To minimize spacing heterogeneity, all the images were taken at the focal plane where the area of the nuclei was largest. Statistical analyses were performed with Image J software and at least 50 independent trichomes of each genotype were used. All experiments were repeated three times and the results displayed same trends. Student's t-test was used to assess the difference between WT and mutants.

#### **Drug treatments**

The experiments were conducted according to Mathru and Chua (2000). The seedlings of CS6550 and CS6550 CA-ROP2 were grown on Murashige and Skoog (MS) medium for 3 days, and then were transferred to the MS medium with or without microtubule disrupting drug oryzalin (5 μм) for another 4 days growth. Because the first pair of the true leaves may not grow synchronous among the seedlings, the growth response of trichomes in the first pair of leaves to the drugs may be different. To ensure an accurate comparison, trichomes on the 3rd rosette leaves were used for morphology change assessments. For each treatment, at least 20 seedlings were used, and the experiments were repeated for three times.

#### **ACKNOWLEDGEMENTS**

This work is supported by the National Natural Science Foundation of China (31470290; 32070198), the Chinese Universities Scientific Fund (2452020180), and the U.S. National Science Foundation (1923589). We are also grateful to Prof. Zhenbiao Yang for the generation of CA-ROP2 and DN-ROP2 plants.

# **AUTHOUR CONTRIBUTIONS**

LA and LL conceived the project and designed the experiments. LL, LN, KJ, YW, CZ and MP performed the experiments. LA, LL and WW analyzed the data. LL and LA wrote the manuscript. FY and JS revised the manuscript.

#### **CONFLICT OF INTEREST**

The authors declare no conflict of interest.

# SUPPORTING INFORMATION

Additional Supporting Information may be found in the online version of this article.

Figure S1. Developmental phenotypes of abt3-1 (axr1-32). (a) Root hair phenotypes of 4-day-old MS grown WT and abt3-1 plants. Scale bars = 400  $\mu$ m. (b,c) Statistic analyses of root hair length (b) and root hair numbers (c). (d) Shoot architecture of mature WT and abt3-1 plants. (e) Statistic analyses of plant height of WT and abt3-1. For all quantitative analyses, data were expressed as means  $\pm$  SD ( $n \ge 20$ ). Student's *t*-test was used to assess the difference from WT (\*\*\*\*, P < 0.0001).

Figure S2. Map-based cloning of the ABT3 locus. Bulked segregant analyses with DNA pool constructed by 95 individuals from

the F2 mapping population and 25 pairs of molecular markers that evenly distribute on the five chromosomes of Arabidopsis localized the ABT3 locus to the Chromosome I, nearing the marker F12K11. Green lines represent the chromosomes and red bars indicate the centromeres.

Figure S3. Phenotypic analyses of AXR1 alleles. (a) Schematic representation of the mutation sites in axr1-3 (CS3075). The 5'and 3' untranslated regions were shown as shaded boxes. Open boxes and solid lines represent the exons and introns, respectively. The 5'and 3'untranslated regions were shown as shaded boxes. The exact mutation sites were indicated above the gene model, respectively. (b,c) Overall phenotypes of 2-week-old (b) and 3week-old (c) WT, abt3-1, axr1-3, and abt3-1 × axr1-3 F1 plants. Scale bars = 1 cm for (b) and 2 cm for (c), respectively. (d) Shoot architecture of mature WT, abt3-1, axr1-3, and abt3-1 × axr1-3 F1 plants. (e) Representive trichomes on the fifth rosette leaves of WT, abt3-1, axr1-3, and abt3-1 x axr1-3 F1 plants. Scale bars = 250  $\mu$ m. (f) Quantification of trichome branch numbers on the third rosette leaves of the plants shown in (e) 2/3/4-br for two/ three/four-branched trichomes, respectively. Data were expressed as means  $\pm$  SD. (g) Examination of the AXR1 transcripts levels of WT, abt3-1, and axr1-3 by RT-qPCR. Fold changes were calculated with respect to the expression levels in the WT. Asterisks Student's t-test was used to assess the difference from WT (\*\*\*\*, P < 0.0001, n.s., not significant).

Figure S4. Developmental phenotypes of the abt3-1 pAXR1:AXR1 plants. (a,b) Plant stature of ten-day-old (a) and three-week-old (b) WT, abt3-1, and abt3-1 pAXR1:AXR1 transgenic plants. #1/#5 for independent transgenic lines. Scale bars = 1 cm for (b) and 2 cm for (c), respectively. (c) Shoot architecture of WT, abt3-1, and abt3-1 pAXR1:AXR1 plants. (d) Root hair phenotypes of WT, abt3-1, and abt3-1 pAXR1:AXR1 plants. Scale bars = 400 μm. (e,f) Quantification of root hair length (e) and root hair number (f) of WT, abt3-1, and abt3-1 pAXR1:AXR1 plants. Data were expressed as means  $\pm$  SD ( $n \ge 20$ ). Student's t-test was used to assess the difference from WT (\*\*\*\*, P < 0.0001).

Figure S5. Developmental phenotypes of axr1-3 pAXR1:AXR1-GFP plants. (a) Plant statures of three-week-old WT, axr1-3, and arx1-3 pAXR1:AXR1-GFP plants. #3/#4 for independent transgenic lines. Scale bar = 1 cm. (b) AXR1 transcripts levels in the plants shown in (a). Fold changes were calculated with respect to the expression levels in the WT. Student's t-test was used to assess the difference from WT (\*\*\*\*, P < 0.0001). (c) Localization of AXR1 in axr1-3 pAXR1:AXR1-GFP trichome. The first pairs of leaves were mounted and GFP signals were examined with confocal microscope under the exciting light at 488 nm. Images were acquired using the IQ3.0 imaging workstation software (Andor). Scale bars = 20  $\mu$ m. The white arrows indicate the trichome nuclei.

Figure S6. Trichome phenotypes of DN-ROP2 mutant. (a) Representive trichomes on the fifth leaves of WT and DN-ROP2 mutant. Scale bars = 250  $\mu$ m. (b) Quantification of trichome branch numbers on the third leaves of WT and DN-ROP2 plants. Data were expressed as means  $\pm$  SD.

Figure S7. Plant stature of p35S:AXR1-GFP CA-ROP2. Three-weekold plants of WT, p35S:AXR1-GFP, CA-ROP2, and p35S:AXR1-GFP CA-ROP2. p35S:AXR1-GFP CA-ROP2 showed similar leaf morphology to that of CA-ROP2 plants. Scale bar = 1 cm.

Figure S8. Effects of 26S proteasome activities on ROP2 protein fluctuation. (a) Protoplast-based degradation assay of ROP2 in WT. Protoplasts from WT expressing p35S:ROP2-GFP plasmid were treated with CHX and MG132 over the indicated time course and total protein were extracted. ROP2 levels were detected through immuno-blotting with anti-GFP antibody. The amount of PBA1 was used as loading control. (b) Relative expression levels of ROP2. Data were presented as mean  $\pm$  SD of three biological replicates.

Figure S9. Effects of auxin on trichome branching. (a) The hypocotyl phenotypes of 10-day-old YUC2 overexpression plants grown in the light condition. The transgenic plants displayed remarkable long hypocotyls which is the typical characteristic of elevated auxin levels. Scale bar = 0.5 cm. (b) Quantification of the hypocotyl length of plants in different genotypes. (c) Representive trichomes on the fifth rosette leaves of 3-week-old WT, YUC2 overexpression plants, and tir1-10. Scale bars = 250  $\mu$ m. (d) Quantification of the trichome branch numbers on the third rosette leaves of plants shown in (c). 2/3/4-br for 2-/3-/4-branched trichomes, respectively. For all statistical analyses, data were presented as mean  $\pm$  SD. Student *t*-tests were used to indicate significant differences from WT (n.s. not significant, \*\*\*\*, P < 0.0001).

Figure S10. Analyses of trichome nuclei size in axr1 mutants. (a) DAPI staining of trichome nuclei in WT and axr1 mutants. The right panel were enlarged pictures of the boxed parts in the middle panels merged with DIC images. Scale bars = 25 μm. (b) Quantification of the trichome nuclei size with Image J program. Data were shown as mean  $\pm$  SD. Student's  $\emph{t}$ -tests were used to indicate significant differences from WT (\*\*\*\*, P < 0.0001).

Figure S11. Response of CA-ROP2 trichome to oryzalin treatments. (a) Representative trichome morphologies of WT and CA-ROP2 plants under oryzalin treatments. Scale bars = 50 μm. (b) Cortical microtubule (cMTs) organization under oryzalin treatments. Spining-disk confocal microscopy was employed to examine the microtubule arrays with an excitation wavelength at 488 nm. Scale bars =  $50 \mu m$ .

Figure S12. Working model of AXR1-ROP2 module in regulating trichome morphogenesis. AXR1-dependent RUB1 modification of SCF ubiquitin ligase mediates ROP2 degradation and formal trichome morphogenesis. Functional loss of AXR1 inactivates SCF ubiquitin ligase and ROP2 accumulation, further leading to the formation of hypo-branched trichomes.

Table S1. The primer pairs used in this work.

# **OPEN RESEARCH BADGES**



This article has earned Open Data and Open Materials badges. Data and materials are available at https://onlinelibrary.wiley.com/ journal/1365313x.

#### REFERENCES

- Chai, S., Ge, F., Feng, Q., Li, S. & Zhang, Y. (2016) PLURIRETALA mediates ROP2 localization and stability in parallel to SCN1 but synergistically with TIR1 in root hairs. The Plant Journal, 86, 413-425.
- Chalvin, C., Drevensek, S., Dron, M., Bendahmane, A. & Boualem, A. (2020) Genetic control of glandular trichome development. Trends in Plant Science, 5, 477-487.
- Chen, X., Grandont, L., Li, H., Hauschild, R., Paque, S., Abuzeineh, A. et al. (2014) Inhibition of cell expansion by rapid ABP1-mediated auxin effect on microtubules. Nature, 516, 90-93.
- Clough, S.J. & Bent, A.F. (1998) Floral dip: a simplified method for agrobacterium-mediated transformation of Arabidopsis thaliana. The Plant Journal, 16, 735-743.
- del Pozo, J.C., Boniotti, M.B. & Gutierrez, C. (2002) Arabidopsis E2FC functions in cell division and is degradaed by the ubiquitin-SCFAtSKP2 pathway in response to light. The Plant Cell, 14, 3057-3071.
- del Pozo, J.C., Dharmasiri, S., Hellmann, H., Walker, L., Gray, W.M. & Estelle, M. (2002) AXR1–ECR1–dependent conjugation of RUB1 to the Arabidopsis Cullin AtCUL1 is required for auxin response. The Plant Cell, 14, 421-433.

- Estelle, M.A. & Somerville, C. (1987) Auxin-resistant mutants of Arabidopsis thaliana with an altered morphology. Molecular and General Genetics, **206**. 200–206.
- Fambrini, M. & Pugliesi, C. (2019) The dynamic genetic-hormonal regulatory network controlling the trichome development in leaves. Plants, 8, 253.
- Friml, J., Gallei, M., Gelová, Z., Johnson, A., Mazur, E., Monzer, A. et al. (2022) ABP1-TMK auxin perception for global phosphorylation and auxin canalization. Nature, 609, 575-581.
- Fu, Y., Gu, Y., Zheng, Z., Wasteneys, G. & Yang, Z. (2005) Arabidopsis interdigitating cell growth requires two antagonistic pathways with opposing action on cell morphogenesis. Cell, 120, 687-700.
- Fu, Y., Li, H. & Yang, Z. (2002) The ROP2 GTPase controls the formation of cortical fine F-actin and the early phase of directional cell expansion during Arabidopsis organogenesis. The Plant Cell, 14, 777-794.
- Gao, Y., Zhang, Y., Zhang, D., Dai, X., Estelle, M. & Zhao, Y. (2015) Auxin binding protein 1 (ABP1) is not required for either auxin signaling or Arabidopsis development. Proceedings of the National Academy of Sciences of the United States of America, 112, 2275-2270.
- Grav. W.M., del Pozo, J.C., Walker, L., Hobbie, L., Risseeuw, E., Banks, T. et al. (1999) Identification of an SCF ubiquitin ligase complex required for auxin response in Arabidopsis thaliana. Genes & Develoment, 13, 1678-1691.
- Han, G., Li, Y., Yang, Z., Wang, C., Zhang, Y. & Wang, B. (2022) Molecular mechanisms of plant trichome development. Frontiers in Plant Science,
- Hülskamp, M. (2004) Plant trichomes: a model for cell differentiation. Nature Reviews Molecular Cell Biology, 5(6), 471-480.
- Hülskamp, M., Misera, S. & Jurgens, G. (1994) Genetic dissection of trichome cell development in Arabidopsis. Cell, 76, 555-566.
- Igisch, C.P., Miège, C. & Jaillais, Y. (2022) Cell shape: a ROP regulatory tugof-war in pavement cell morphogenesis. Current Biology, 32, R116-R140.
- Ishida, T., Kurata, T., Okada, K. & Wada, T. (2008) A genetic regulatory network in the development of trichomes and root hairs, Annual Review of Plant Biology, 59, 365-386.
- Kang, E., Zheng, M., Zhang, Y., Yuan, M., Yalovsky, S., Zhu, L. et al. (2017) The microtubule-associated protein MAP18 affects ROP2 GTPase activity during root hair growth, Plant Physiology, 174, 202-222,
- Leyser, H.M.O., Lincoln, C.A., Timpte, C., Lammer, D., Turner, J. & Estelle, M. (1993) Arabidopsis auxin resistance gene AXR1 encodes a protein related to ubiquitin-activating enzyme E1. Nature, 364, 161-164.
- Leyser, O. (2018) Auxin signaling. Plant Physiology, 176, 465-479.
- Li, C., Lu, H., Li, W., Yuan, M. & Fu, Y. (2017) A ROP2-RIC1 pathway finetunes microtubule reorganization for salt tolerance in Arabidopsis. Plant, Cell and Environment, 40, 1127-1142.
- Li, H., Shen, J.J., Zheng, Z.L., Lin, Y. & Yang, Z. (2001) The Rop GTPase switch controls multiple development processes in Arabidopsis. Plant Physiology, 126, 670-684.
- Li, L., Verstraeten, I., Roosjen, M., Takahashi, K., Rodriguez, L., Merrin, J. et al. (2021) Cell surface and intracellular auxin signaling for H<sup>+</sup> fluxes in root growth. Nature, 599, 273-277.
- Li, P., Fu, J., Xu, Y., Shen, Y., Zhang, Y. & Ye, Z. (2022) CsMYB1 integrates the regulation of trichome development and catechins biosynthesis in tea plant domestication. New Phytologist, 234, 902-917.
- Li, Y., Kurepa, J. & Smalle, J. (2013) AXR1 promotes the Arabidopsis cytokinin response by facilitating ARR5 proteolysis. The Plant Journal, 74, 13-24.
- Liang, S., Yang, X., Deng, M., Zhao, J., Shao, J., Qi, Y. et al. (2019) A new allele of the SPIKE1 locus reveals distinct regulation of trichome and pavement cell development and plant growth. Frontiers in Plant Science, **10**, 16.
- Lin, D., Cao, L., Zhou, Z., Zhu, L., Ehrhardt, D., Yang, Z. et al. (2013) Rho GTPase signaling activates microtubule severing to promote microtubule ordering in Arabidopsis. Current Biology, 23, 290-297.
- Lin, D., Ren, H. & Fu, Y. (2015) ROP GTPase-mediated auxin signaling regulates pavement cell interdigitation in Arabidopsis thaliana. Journal of Integrative Plant Biology, 57, 31-39.
- Lin, W., Zhou, X., Tang, W., Takahashi, K., Pan, X., Dai, J. et al. (2021) TMKbased cell-surface auxin signaling activates cell-wall acidification. Nature, 599, 278-282.
- Lincoln, C., Britton, J.H. & Estelle, M. (1990) Growth and development of the axr1 mutants of Arabidopsis. The Plant Cell, 2, 1071-1080.

- Liu, S., Jobert, F., Rahneshan, Z., Doyle, S.M. & Robert, S. (2021) Solving the puzzle of shape regulation in plant epidermal pavement cells. Annual Review of Plant Biology, 72, 525-550.
- Lukowitz, W., Gillmor, C.S. & Scheible, W.R. (2000) Positional cloning in Arabidopsis. Why it feels good to have a genome initiative working for you. Plant Physiology, 123, 795-805.
- Martinez-Garda, M., Fernández-Jiménez, N., Santos, J.L. & Pradillo, M. (2020) Duplication and divergence: new insight into AXR1 and AXL functions in DNA repair and meiosis. Scientific Reports, 10, 8860.
- Masucci, J.D. & Schiefelbein, J.W. (1996) Hormones act downstream of TTG and GL2 to promote root hair outgrowth during epidermis development in the Arabidopsis root. The Plant Cell, 8, 1505-1517.
- Mathru, J. & Chua, N. (2000) Microtubule stabilization leads to growth reorientation in Arabidopsis trichomes. The Plant Cell, 12, 465-477.
- Matias-Hernandez, L., Jiang, W., Yang, K., Tang, K., Brodelius, P.E. & Pelaz, S. (2017) AaMYB1 and its orthologue AtMYB61 affect terpene metabolism and trichome development in Artemisia annua and Arabidopsis thaliana. The Plant Journal, 90, 520-534.
- Nagawa, S., Xu, T. & Yang, Z. (2010) RHO GTPase in plants: conservation and invention of regulators and effectors. Small GTPases, 1, 78-88.
- Ou, H. & Yi, P. (2022) ROP GTPase-dependent polarity establishment during tip growth in plants. New Phytologist, 236, 49-57.
- Ren, H., Dang, X., Yang, Y., Huang, D., Liu, M., Gao, X. & Lin, D. (2016)SPIKE1 activates ROP GTPase to modulate petal growth and shape. Plant Physiology, 172, 358-371.
- Ren, H., Santner, A., del Pozo, J.C., Murray, J.A.H. & Estelle, M. (2008) Degradation of the cyclin-dependent kinase inhibitor KRP1 is required by two different ubiquitin E3 ligase. The Plant Journal, 53, 705-716.
- Robinson, D.O. & Roeder, A.H. (2015) Themes and variations in cell type patterning in the plant epidermis. Current Opinion in Genetics & Development, 32, 55-65.
- vRuegger, M., Dewey, E., Gray, W.M., Hobbie, L., Turner, J. & Estelle, M. (1998) The TIR1 protein of Arabidopsis functions in auxin response and is related to human SKP2 and yeast Grr1p. Genes & Development, 12, 198-207
- Schnittger, A. & Hülskamp, M. (2002) Trichome morphogenesis: a cell-cycle perspective. Philosophical Transactions of the Royal Society B: Biological Sciences, 29, 823-826.
- Schnittger, A., Weinl, C., Bouyer, D., Schöbinger, U. & Hülskamp, M. (2003) Misexpression of the cyclin-dependent kinase inhibitor ICK1/KRP1 in single-celled Arabidopsis trichomes reduces endoreduplication and cell size and induces cell death. The Plant Cell, 15, 303-315.
- Schwab, B., Folkers, U., Ilgenfritz, H. & Hülskamp, M. (2000) Trichome morphogenesis in Arabidopsis. Philosophical Transactions of the Royal Society B: Biological Sciences, 355, 879-883.
- Schwechheimer, C., Serino, G. & Deng, X. (2002) Multiple ubiquitin ligasemediated processes required COP9 signalosome and AXR1 function. The Plant Cell, 14, 2553-2563.
- Shang, X., Cao, Y. & Ma, L. (2017) Alternative splicing in plant genes: a means of regulating the environmental fitness of plants. International Journal of Molecular Science, 18, 432.
- Szymanski, D. & Marks, M.D. (1998) GLABROUS1 overexpression and TRYPTYCHON alter the cell cycle and trichome cell fate in Arabidopsis. The Plant Cell, 10, 2047-2062.
- Tirvaki, I. & Staswick, P. (2002) An Arabidopsis mutant defective in jasmonate response is allelic to the auxin-signaling mutant axr1. Plant Physiology, 130, 887–894.
- Tominaga-Wada, R., Ishida, T. & Wada, T. (2011) New insights into the mechanism of development of Arabidopsis root hairs and trichomes. International Review of Cell and Molecular Biology, 286, 67-106.
- Wang, F., Zhu, D., Huang, X., Li, S., Gong, Y., Yao, Q. et al. (2009) Biochemical insights on degradation of Arabidopsis DELLA proteins gained from a cell free assay system. The Plant Cell, 21, 2378-2390.
- Wang, J., Guo, X., Xiao, Q., Zhu, J., Cheung, A., Yuan, L. et al. (2020) Auxin efflux controls orderly uncellar degeneration and expansion of the female gametophyte in Arabidopsis. New Phytologist, 230, 2261-
- Wang, S., Barron, C., Schiefelbein, J. & Chen, J. (2010) Distinct relationships between GLABRA2 and single-repeat R3 MYB transcription factors in the regulation of trichome and root hair patterning in Arabidopsis. New Phytologist, 185, 387-400.

- Wang, X., Shen, C., Meng, P., Tan, G. & Lv, L. (2021) Analysis and review of trichomes in plants. *BMC Plant Biology*, **21**, 70.
- Wang, Z., Yang, Z. & Li, F. (2019) Updates on molecular mechanisms in the development of branched trichome in Arabidopsis and nonbranched in cotton. *Plant Biotechnology Journal*, 17, 1706–1722.
- Xu, T., Dai, N., Chen, J., Nagawa, S., Cao, M., Li, H. et al. (2014) Cell surface ABP1-TMK-auxin-sensing complex activates ROP GTPase signaling. Science, 343, 1025–1028.
- Xu, T., Wen, M., Nagawa, S., Fu, Y., Chen, J. & Wu, M. (2010) Cell surface and Rho GTPasebased auxin signaling controls cellular interdigitation in Arabidopsis. *Cell*, 143, 99–110.
- Yang, Y., Huang, W., Wu, E., Lin, C., Chen, B. & Lin, D. (2019) Cortical microtubule organization during petal morphogenesis in Arabidopsis. *International Journal of Molecular Science*, 20, 4913.
- Yoo, S.D., Cho, Y.H. & Sheen, J. (2007) Arabidopsis mesophyll protoplasts: a versatile cell system for transient gene expression analysis. *Nature Protocols*. 2, 1565–1572.
- Yu, Y., Tang, W., Lin, W., Li, W., Zhou, X., Zhou, X. et al. (2022) ABLs and TMKs are co-receptors for extracellular auxin. bioRxiv preprint https://doi.org/10.1101/2022.11.28.518138
- Zhang, M., Zheng, X., Song, S., Zeng, Q., Hou, L. & Li, D. (2011) Spatio-temporal manipulation of auxin biosynthesis in cotton ovule epidermal cells enhances fiber yield and quality. *Nature Biotechnology*, 29, 453–458.